

# Anisotropic optical response of arthropods's cuticle

L.A.Rodríguez<sup>1</sup>, H.C. Achitte Schmutzler<sup>2</sup>, M.I. Dufek<sup>2</sup>,  
Guillermo P.Ortiz<sup>1</sup>, and W. Luis Mochán<sup>3</sup>

<sup>1</sup>Dpto. Física, Fac. Cs. Exactas, Nat. y A., Univ. Nacional del  
Nordeste,Ctes, Argentina

<sup>2</sup>Dpto. Biología, Fac. Cs. Exactas, Nat. y A., Univ. Nacional del  
Nordeste,Ctes, Argentina

<sup>3</sup>Instituto Cs. Físicas, Univ. Nacional Autónoma de México,  
Cuer., Mor., México

February 25, 2023

## Abstract

The structure of arthropods cuticle consists of layers of microfilamentary chitin particles. The layers are stacked one on top of the other performing an helical (Bouligand helix) pattern. This cuticle structure generate optical phenomena such as structural color and birefringence that develop as metallic appearance or iridescence and polarized reflectance or optical activity. We model the anisotropic optical responses of arthropods cuticle using `Photonic` package to obtain the macroscopic dielectric tensor of a constitutive layer in the Bouligand helix. We found the anisotropy of that dielectric tensor depends on chitin particle shape, reticular arrangement and filling fractions. As a main result, we obtained a cuticle model with tunable reflectance band gaps that are very sensitive to such geometrical parameters and to  $\theta$  angle that controls the helix pitch. We can explain structural color based on the reflectance band gap introduced by anisotropy and its shifts mediated by  $\theta$  instead of as usual approach that consider multiple arrangement of layers pairs with different thickness and optical properties.

## 1 Introduction

There are several structured cuticle that behave like complex photonic crystals generating optical phenomena in sclerotized integument of arthropods like structural color, luminescence, ultraviolet signals, polarized reflectance, and depolarization [1, 2, 3, 4]

The basic model of a stratified cuticle arranged parallel in multilayered structure that can alternates high and low refractive indices, i.e. a Bragg mirror, was broadly used to explain[5, 6, 7] colorful iridescent bright reflection due to constructive/destructive wavelength superposition by interference phenomena.

Also, sections of samples of the dorsal cuticles analyzed with SEM and TEM images confirms the evidence of cuticle structure of the stratified type in several different arthropods [8, 9]. Of course, a Bragg mirrors arrangement only does not can explain more specific optical responses such as the optical activity. When the circular polarized light rotates following the same counterclockwise, it is called right circular polarization and otherwise is left circular polarization [10]. Several beetle species reflect circular polarized light also the marine stomatopod *Odontodactylus scyllarus* and several species of firefly [11, 12]

The typical structure of the cuticle in arthropods consists of layers of chitin microfilamentary particles into protein matrix [9]. The chitin microfilaments are arranged parallel and into helical layers throughout the cuticle behaving similarly to liquids crystals in cholesteric phases[1, 13], it means that particles have a same orientation in a thin layer but stratified and progressively changing its orientation rotating around the layer normal directions deploying an helix structure. The helical model proposed by Bouligand[13], was assumed [1] and later demonstrated [14, 4] that the cuticle is composed of layer with a successive, counterclockwise helical rotation of suitable pitch, i.e. the length traveled along the helix axes for a full rotation around such axes. Due to elongated shape of chitin particles in a layer it has a *form* birefringence properties. The birefringence is the optical property of a material that has different refractive indices to light rays. Crystals of calcite are a very well known example displaying this property. Due to axial symmetry in the molecular arrangement into the crystalline structure the birefringence of the calcite is an intrinsic property[15]. The form birefringence is an important feature of the individual layers, as it contributes to the *strength* of the helix[12]. It is related to the anisotropy that could be due to the aspect ratio of chitin microfilaments or more accurately due to depolarization factor that depend on particle geometry shape and materials. For large differences from one to another of the depolarization factor corresponding to two of its principal axis, larger is the anisotropy, and thus layers constitutes to an helix structures optically stronger.

The Bouligand structures served as the basis for explaining the chitin structure and organization, also to estimate the birefringence and anisotropy from many crustaceans and insects. The polarization of the cuticle structure in insect was studied and looked as a simple model of the reflection mechanism [12]. To know the possible structural origins of the reflection spectra of circular polarized light in beetle cuticle in Ref.[12] is compared the observed spectra in beetle cuticle with spectra modeled as a multilayer transfer matrix method using the Birefringent Thin Films Toolbox (BTFT) [16]. In the BTFT method the form birefringence is estimated through a proposed structure function that perform a mix of voids and chitin's particles with cylindrical shape using the Bragg-Pippard analytical formula[17] to approximate the macroscopic dielectric permittivity of chitin microfilaments composite media. In that model the authors introduced some parameters determined by fitting against data obtained from reflectance measurements which means that they do not model the anisotropy indeed.

In this work, we propose to obtain the anisotropic optical response of a chitin microfilaments layer by calculating their macroscopic dielectric tensor from which and using matrix transfer method we get the reflectance of the cuticle structure. Thanks to this procedure we can explain the reflectance features of the structural color observed in beetles like in Ref.[6, 8] in another way.

The reflectance band gap and also its shifts are produced by anisotropy that is mediated by microstructure details and the helix pitch instead of the often approach considering multiple arrangement of layers pairs with different optical properties and thickness.

We organize this work introducing in Sec.2 the theory and methods to describe calculation of the macroscopic dielectric tensor for a layer of chitin microfibrils particle. In Subsec.2.1 we resume an appropriate transfer matrix method that we used in Subsec.2.2 to obtain the cuticle anisotropic reflectance. In Sec.3 we present and discuss the results we found, and Sec.4 is devoted to our conclusion.

## 2 Theory and Methods

We want to model the optical response of a layered system with total thickness  $L$  where each layer is constituted by intertwined chitin macromolecules developing a planar array of elongated microfibrillary particles with cross section of a few nm in diameters. In these layers exists a preferential direction defined by the alignment in average of the major axes of the microfibrillary particles. However, each layer has a different average alignment direction and thus we chose the laboratory system reference to describe the optical response of the whole layered structure. We model the optical response of each layer using Photonic and employing a transfer matrix method to obtain the reflectance  $R$  and transmittance  $T$  of the total system.

Fig. 1 displays an scheme of the progressive rotated  $M$  layers developing an helical Bouligand structure [13]. Layers are stacked and successively rotated counterclockwise in  $\theta$ . They are defined for a simple example with thirty parti-

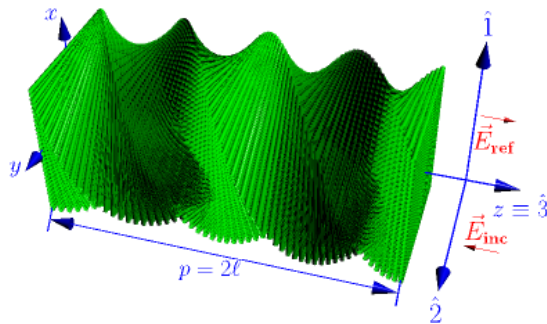


Figure 1: Bouligand structure scheme for  $M = 73$  stacked layers progressive rotated each in  $\theta = 5$  around  $z$  axes in the laboratory reference frame  $x, y, z$  with helix pitch  $p$  and period  $\ell$ . Fields  $\vec{E}_{\text{inc}}$  and  $\vec{E}_{\text{ref}}$  for an incident probe beam and its reflection in the  $z$  axes direction of the laboratory reference and equal to axes  $\hat{z}$  belonging to body frame reference with principal axis  $\hat{1}$  and  $\hat{2}$ .

cles of cylindrical shape with aspect ratio height to diameter of thirty arranged side by side forming a squared base. The helix pitch is  $p$  and due to a half of full rotation symmetry of cylindrical particles around the normal to its axes the Bouligand structure has a period  $\ell = p/2$ . Normal incidence of a probe beam is taken at normal direction of layers which named  $\hat{z}$  in the laboratory frame

$(\hat{x}, \hat{y}, \hat{z})$  and equivalent to axes  $\hat{3}$  in the body reference frame  $(\hat{1}, \hat{2}, \hat{3})$ .

Fig. 2 displays at the left a zoom of Fig. 1 indicating some  $M$  layers of

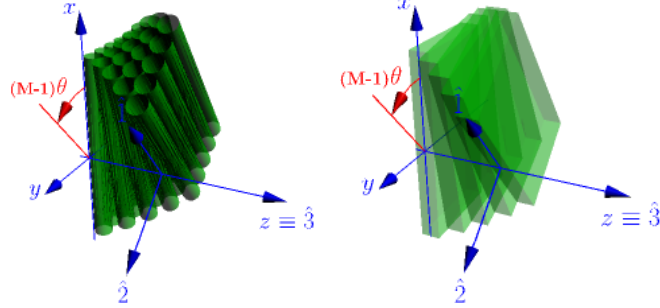


Figure 2: Left: Details of Fig.1 for cylindrical chitin particles. Right: Scheme substituting particles specific geometry with homogeneous slabs that allows us to model anisotropic response calculated with **Photonic**. There are principals axis in layers planes  $\hat{1}$ ,  $\hat{2}$  and the respective laboratory axis  $x$ ,  $y$ . The  $z$  and  $\hat{3}$  axis are the same. The progressive rotation  $(M - 1)\theta$  follows for each of  $1 \dots M$  layers.

cylinders progressively rotatated in  $\theta$ . In the right part of Fig. 2 the  $M$  layers of cylinders are substituted by  $M$  homogeneous slabs corresponding each to the macroscopic dielectric tensor obtained using **Photonic** [18]. As expected, it is diagonal in the body frame  $(\hat{1}, \hat{2}, \hat{3})$  and we write the parallel part

$$\epsilon_{\parallel}^M = \begin{pmatrix} \epsilon_{11} & 0 \\ 0 & \epsilon_{22} \end{pmatrix} \quad (1)$$

As usual, we use a linear transformation of rotation in the layer plane to obtain  $\epsilon_{\parallel}$  in the laboratory frame

$$\epsilon_{\parallel}^M = \begin{pmatrix} \epsilon_{xx} & \epsilon_{xy} \\ \epsilon_{yx} & \epsilon_{yy} \end{pmatrix}, \quad (2)$$

and it is always symmetric  $\epsilon_{xy} = \epsilon_{yx}$ . Fig. 3 displays the geometries and the particles section views with the lattice unit cells we have explored. Note that for clearness in the schema of the cuticle structure we put only one cylinder stack in each layer shows in Fig.2 left panel. But, we expect that there could be a bunch of chitin particles more or less aligned and that units cells cuts displayed in Fig.3 allows a good enough representation of each layer for the calculation of macroscopic dielectric tensor responses. Fig.3 displays in upper (lower) panel square (triangular) unit cells  $(\hat{2}, \hat{3})$  frame body cuts directions tiled  $3 \times 3$  times. In the left (right) panel of Fig.3 for cylindrical (hexagonal) particles section with  $f = 0.75$  ( $f = 0.6$ ) approximately to the maximum filling fractions for the square lattice. Note that for triangular lattices a larger  $f$  values are allowed due to the smaller unit cell surface in such cases. With numerical computation via **Photonic** there are parameter  $N$  and  $N_h$  that need to be tested for witness of convergence. The  $2N + 1$  point per unit cells side are used to define the particle geometry, while  $N_h$  define the number of states used to represent physical objects in the Fourier space for Haydock recursion method[18].

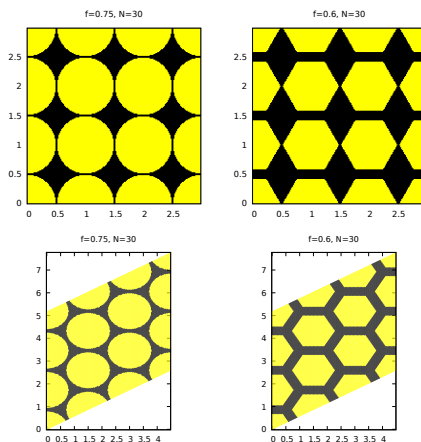


Figure 3: Upper (Lower) panels shows tiled  $3 \times 3$  times square (triangular) unit cells cuts for  $(\hat{2}, \hat{3})$  frame body directions. In the left (right) for cylindrical (hexagonal) particles sections for  $f = 0.75$  ( $f = 0.6$ ) filling fractions. There are  $2N + 1$  points by unit cells side used for the particle geometry definition.

From the self-consistent fields obeying Maxwell Eqs. we may obtain the optical response of the layered system. We first suppose that exist two waves inside of each layer with wavevectors  $\vec{k} = \pm \frac{\omega}{c} n \hat{z}$ , with  $n$  depending on dielectric tensor components. Note that for isotropic materials  $n = \sqrt{\epsilon}$  with  $\mu = 1$  and  $\epsilon$  the permittivity media. For anisotropic media  $n$  is obtained from the dispersion relation. Alternatively, we may proceed applying Faraday and Ampere-Maxwell Eqs. in the laboratory frame reference to obtain from  $\vec{E}$  and  $\vec{H}$  the named *continuous vector*  $(E_x, H_y, E_y, H_x)$  [16] corresponding to parallels components  $\vec{E}_{\parallel}$  and  $\vec{H}_{\parallel}$  to the layers interfaces, which must obeys

$$\begin{pmatrix} 0 & 1 & 0 & 0 \\ \epsilon_{xx} & 0 & \epsilon_{xy} & 0 \\ 0 & 0 & 0 & -1 \\ -\epsilon_{xy} & 0 & -\epsilon_{yy} & 0 \end{pmatrix} \begin{pmatrix} E_x \\ H_y \\ E_y \\ H_x \end{pmatrix} = n \begin{pmatrix} E_x \\ H_y \\ E_y \\ H_x \end{pmatrix} \quad (3)$$

eigenvalues and eigenvectors equations. The characteristic polynomial give us 4 solutions for  $n$

$$n^2 = \frac{\epsilon_{xx} + \epsilon_{yy}}{2} \pm \frac{1}{2} \sqrt{(\epsilon_{xx} - \epsilon_{yy})^2 + 4\epsilon_{xy}^2} \quad (4)$$

which we may easily identify as is diagonal case with solutions  $n_1^{\pm} = \pm \sqrt{\epsilon_{11}}$  and  $n_2^{\pm} = \pm \sqrt{\epsilon_{22}}$  corresponding to the two sets of counter propagating waves normal modes of each layer.

## 2.1 Transfer matrix M for anisotropic system

Here we briefly resume well known theory for propagating field Maxwell Eqs. solutions in stratified media [19], but instead to follow the backward fields transfer description [16, 19] we will describe a forward fields transfer like in Ref. [20, 21],

because the last ones follows straightforwardly. From  $\vec{E}_{\parallel}$  and  $\vec{H}_{\parallel}$  we write the continuous vector in terms of the eigenvectors  $\{\vec{v}_1^+, \vec{v}_1^-, \vec{v}_2^+, \vec{v}_2^-\}$ , as

$$\begin{pmatrix} E_x \\ H_y \\ E_y \\ H_x \end{pmatrix} = \gamma_1^+ \vec{v}_1^+ + \gamma_1^- \vec{v}_1^- + \gamma_2^+ \vec{v}_2^+ + \gamma_2^- \vec{v}_2^- \quad (5)$$

using the complex amplitudes  $\gamma_1^{\pm}$  and  $\gamma_2^{\pm}$ . Introducing matrix  $\mathbf{B}$  made up with columns of that eigenvectors, thus  $\mathbf{B}$  only depends on the layer permittivity tensor components. In any plane  $z$  inside each layer, the amplitudes from laboratory frame can be obtained

$$\begin{pmatrix} \gamma_1^+ \\ \gamma_1^- \\ \gamma_2^+ \\ \gamma_2^- \end{pmatrix}_z = \mathbf{B}^{-1} \begin{pmatrix} E_x \\ H_y \\ E_y \\ H_x \end{pmatrix}_z \quad (6)$$

Note from (5) that we can assign to the amplitudes of each eigenvectors the phase  $\pm k_0 n_i z$  with  $i = 1, 2$  and  $k_0 = \omega/c$  as function of the  $z$  position propagation coordinates, thus we may write for  $z_1 < z < z_2$

$$\begin{pmatrix} \gamma_1^+ \\ \gamma_1^- \\ \gamma_2^+ \\ \gamma_2^- \end{pmatrix}_{z=z_2} = \mathbf{P}(z_2 - z_1) \begin{pmatrix} \gamma_1^+ \\ \gamma_1^- \\ \gamma_2^+ \\ \gamma_2^- \end{pmatrix}_{z=z_1} \quad (7)$$

where

$$\mathbf{P}(z) = \begin{pmatrix} e^{ik_0 n_1 z} & 0 & 0 & 0 \\ 0 & e^{-ik_0 n_1 z} & 0 & 0 \\ 0 & 0 & e^{ik_0 n_2 z} & 0 \\ 0 & 0 & 0 & e^{-ik_0 n_2 z} \end{pmatrix} \quad (8)$$

Using (7) and (6) we obtain the continuous vector transformation from  $z = z_1$  to  $z = z_2$  positions

$$\begin{pmatrix} E_x \\ H_y \\ E_y \\ H_x \end{pmatrix}_{z=z_2} = \mathbf{BP}(z_2 - z_1)\mathbf{B}^{-1} \begin{pmatrix} E_x \\ H_y \\ E_y \\ H_x \end{pmatrix}_{z=z_1} \quad (9)$$

For a layer of thickness  $d$  with its left interface at  $z = z_0$ ,  $\mathbf{M}(d) = \mathbf{BP}(d)\mathbf{B}^{-1}$  allows us to obtain the transformation of continuous vector from  $z = z_0$  to  $z = z_0 + d$

$$\begin{pmatrix} E_x \\ H_y \\ E_y \\ H_x \end{pmatrix}_{z=z_0+d} = \mathbf{M}(d) \begin{pmatrix} E_x \\ H_y \\ E_y \\ H_x \end{pmatrix}_{z=z_0} \quad (10)$$

Then, for a layered system with thickness  $L$  like in Fig.2 with its first interface in  $z = 0$ , and with  $N$  contiguous layers each one of width  $d_i$  and  $i = 1 \dots N$ , we

obtain

$$\begin{pmatrix} E_x \\ H_y \\ E_y \\ H_x \end{pmatrix}_{z=L} = \mathbf{M} \begin{pmatrix} E_x \\ H_y \\ E_y \\ H_x \end{pmatrix}_{z=0} \quad (11)$$

where  $L = \sum_i^N d_i$  and  $\mathbf{M} = \mathbf{M}_N(d_N)\mathbf{M}_{N-1}(d_{N-1}) \dots \mathbf{M}_1(d_1)$  defines the *transfer matrix* of the whole system.

## 2.2 Reflection coefficients for anisotropic system

Note that in (11) we have the total parallel field components to the interfaces at  $z = 0$  and at  $z = L$ . Thus, for the incident and reflected fields at  $z = 0$  and for the transmitted field at  $z = L$ , we can write

$$\begin{pmatrix} E_{tx} \\ H_{ty} \\ E_{ty} \\ H_{tx} \end{pmatrix}_{z=L} = \mathbf{M} \begin{pmatrix} E_{0x} + E_{rx} \\ H_{0y} + H_{ry} \\ E_{0y} + E_{ry} \\ H_{0x} + H_{rx} \end{pmatrix}_{z=0}. \quad (12)$$

Also, note that as the incident and transmitted media are isotropic, we have  $H_{tx} = E_{ty}/Z_s$  and  $H_{ty} = E_{tx}/Z_s$  at  $z = 0$ , while  $H_{0x} + H_{rx} = (E_{0y} - E_{ry})/Z_0$  and  $H_{0y} + H_{ry} = (E_{0x} - E_{rx})/Z_0$  at  $z = L$ , where  $Z_i = 1/n_i$  are impedance for normal incidence and  $n_0, n_s$  refractive index for incident medium and substrate medium. Such relations allows us to equate a pair of transmitted fields expressions to reduce from  $4 \times 4$  to one of  $2 \times 2$  Eqs. system. After a simple algebra and rearranging terms, we can write

$$\mathbf{M}_1 \begin{pmatrix} E_{0x} + E_{rx} \\ (E_{0x} - E_{rx})/Z_0 \end{pmatrix} = \mathbf{M}_2 \begin{pmatrix} E_{0y} + E_{ry} \\ (E_{0y} - E_{ry})/Z_0 \end{pmatrix}, \quad (13)$$

where

$$\mathbf{M}_1 = \begin{pmatrix} m_{11} - Z_S m_{21} & m_{12} - Z_S m_{22} \\ m_{31} - Z_S m_{41} & m_{32} - Z_S m_{42} \end{pmatrix}, \quad (14)$$

and

$$\mathbf{M}_2 = \begin{pmatrix} Z_S m_{23} - m_{13} & Z_S m_{24} - m_{14} \\ Z_S m_{43} - m_{33} & Z_S m_{44} - m_{34} \end{pmatrix}, \quad (15)$$

with  $m_{ij}$  defined in (11). Finally, reflected fields are

$$\begin{pmatrix} E_{rx} \\ E_{ry} \end{pmatrix} = \mathbf{A}^{-1} [ E_{0x} \mathbf{M}_1 - E_{0y} \mathbf{M}_2 ] \begin{pmatrix} 1 \\ 1/Z_0 \end{pmatrix}, \quad (16)$$

with  $2 \times 2$  matrix

$$\mathbf{A} = \left[ -\mathbf{M}_1 \begin{pmatrix} 1 \\ -1/Z_0 \end{pmatrix} \mathbf{M}_2 \begin{pmatrix} 1 \\ -1/Z_0 \end{pmatrix} \right] \quad (17)$$

From (16) we can obtain the useful anisotropic reflectance coefficients [22]

$$\begin{aligned} r_{xx} &= E_{rx}/E_{0x} \quad (E_{0y} = 0) \\ r_{xy} &= E_{rx}/E_{0y} \quad (E_{0x} = 0) \\ r_{yy} &= E_{ry}/E_{0y} \quad (E_{0x} = 0) \\ r_{yx} &= E_{ry}/E_{0x} \quad (E_{0y} = 0) \end{aligned} \quad (18)$$

### 3 Results

Fig. 4 displays  $\epsilon_{ij}^M$  with  $i = j = 1, 2$  versus  $f$  and the aspect ratio  $e$  corresponding to Eq.(1) and  $e = h/2r$  with particles height  $h$  and radius  $r$ . In the upper (lower) panel for square (triangular) lattice. Left (Right) panels corresponds to cylindrical (hexagonal) particle geometry sections. Convergence of  $\epsilon_{ij}^M$  with  $N$  and  $N_h$  values used are obtained with no appreciable difference above  $N = 30$  and  $N_h = 20$ . Note that differences of  $\epsilon_{ii}^M$  in longitudinal  $\hat{1}\hat{1}$  respect

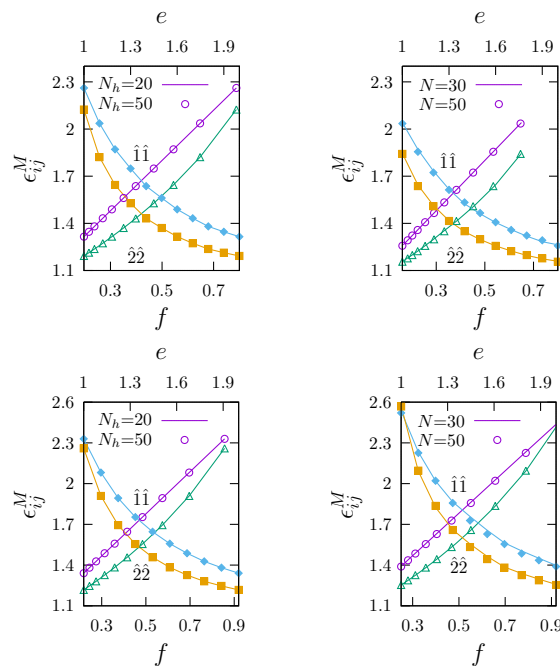


Figure 4: The diagonal macroscopic tensor components  $\epsilon_{ij}^M$   $i = j = 1, 2$  versus  $f$  and the aspect ratio  $e$  for left (right) cylinder (hexagonal) Eq.(1). Upper (Lower) panel square (triangular) lattice cell cases. Linespoints versus continuous line are used to test  $N$  and  $N_h$  convergences with no appreciable differences above  $N = 30$  and  $N_h = 20$ .

to transversal  $\hat{2}\hat{2}$  particles directions corresponds to the form birefringence we have obtained for each modeled layer given by the anisotropic diagonal tensor  $\epsilon_{ij}^M$ . Fig. 5 displays anisotropic reflectance  $R_{ij} = |r_{ij}|^2$  according to Eq.(18) for the free standing ( $Z_0 = Z_s = 1$ ) Bouligand structure with total thickness  $L = 2496$  nm for  $\theta = 10^\circ$  and  $M = 216$  layers of thickness  $d = L/M = 11.56$  nm each one. For cylindrical particles section  $\epsilon_{11}^M = 2.2$ ,  $\epsilon_{22}^M = 2.03$  for square lattice (left upper panel) and  $\epsilon_{11}^M = 2.2$ ,  $\epsilon_{22}^M = 2.0$  for triangular lattice (left lower panel). For hexagonal particles section  $\epsilon_{11}^M = 1.96$ ,  $\epsilon_{22}^M = 1.75$  for square lattice (right upper panel), and  $\epsilon_{11}^M = 1.97$ ,  $\epsilon_{22}^M = 1.74$  for triangular lattice (right lower panel). Note that near to  $\hbar\omega_{\text{cyl}} = 2.05$  eV for cylindrical and near to  $\hbar\omega_{\text{hex}} = 2.19$  eV for hexagonal cases we have the centroid of the band gap  $\langle R \rangle_{\text{bgcp}}$  for the reflectance average  $\langle R \rangle = \frac{1}{2}(R_{xx} + R_{yy})$  for no polarized light as



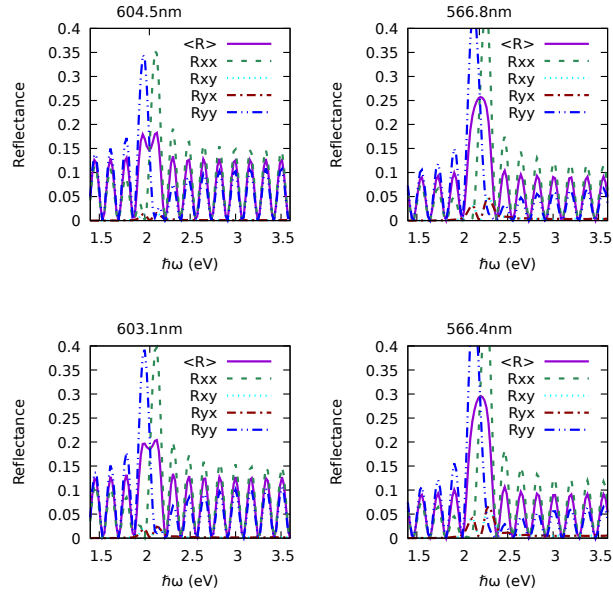


Figure 5: Reflectance  $R_{ij}$  versus photon energy  $\hbar\omega$  in eV for Bouligand structure with thickness  $L = 2496$  nm,  $\theta = 10^\circ$  and  $M = 216$  layers. Cases are ordered as in results of Figs.3 and 4.  $\langle R \rangle_{\text{bgcp}}$  develops at  $\lambda = 604.5$  (566.8) and 603.1nm (566.4) for cylindrical (hexagonal) particle sections. Continuous line for  $\langle R \rangle = \frac{1}{2}(R_{xx} + R_{yy})$ . Dashed lines for  $R_{xx}$ , Dashed dotted-dotted lines for  $R_{yy}$  are one order of magnitude larger than  $R_{xy}$  and  $R_{yx}$  which are displayed in dotted and dashed-dotted lines.

expected for the modeled Bouligand structures[12]

$$1239.8/\hbar\omega = p \frac{\sqrt{\epsilon_{11}} + \sqrt{\epsilon_{22}}}{2}. \quad (19)$$

Note that larger values of  $\epsilon_{ii}^M$  for cylindrical case are also related to the larger  $f$  as well as the larger amplitude of the oscillation outside the band gap compared to the hexagonal case. Note also that as a consequence of larger  $\epsilon^M$  the period of such oscillation is smaller than the respective for hexagonal case. These facts could explain partially only a larger peaks overlap by superposition of  $R_{xx}$  and  $R_{yy}$  in the hexagonal compared to cylindrical case. Also, in Fig. 5  $\langle R \rangle_{\text{bgcp}}$  is larger when the anisotropy difference  $\Delta n = (n_{11} - n_{22})/n_{22}$  increases following  $\Delta n = 0.041, 0.049, 0.058$  and  $0.064$  for left upper, left lower, right upper and right lower panels, respectively. Clearly for  $\Delta n \rightarrow 0$  anisotropy disappear as also any band gap reflectance. The helix strength related to  $\Delta n > 0$  means that constructive interference phenomena takes place and for larger strength larger is the band gap reflectance. Some features of the overlapped peaks depends on  $\theta$  also. Fig.6 displays anisotropic reflectance  $R_{ij}$  for the similar Bouligand

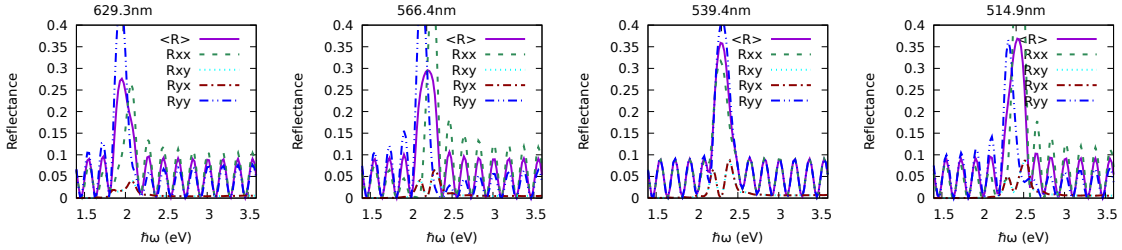


Figure 6: Reflectance  $R_{ij}$  versus photon energy  $\hbar\omega$  in eV for Bouligand structure similar to Fig.5 but only for triangular lattice and hexagonal particles in order from left to right with  $\theta = 9^\circ, 10^\circ, 10.5^\circ$  and  $11^\circ$ . The  $\langle R \rangle_{\text{bgcp}}$  shifts are  $\lambda = 629.3, 566.4, 539.4$  and  $514.9\text{nm}$ , respectively.

structures of Fig.5 but now only for triangular lattice and hexagonal particles with  $\theta = 9^\circ, 10^\circ, 10.5^\circ$  and  $11^\circ$ . Ripples features of the band gap shape related to  $\theta$  has attracted some attention [12] and would be explained here. As  $\theta = 10^\circ$  correspond to six full helix rotation for  $M = 216$ , a compensated contribution of the orthogonal components  $R_{xx}$  and  $R_{yy}$  to  $\langle R \rangle$  is obtained as we can verify from the symmetric reflectance band gap in the second panel of Fig.6. A  $\theta$  value not commensurate with some integer of full helix rotation will give uncompensated contribution as we can see in the others panel of Fig.6. According to Eq.(19) and  $p = 360d/\theta$ , the  $\hbar\omega$  is proportional to  $\theta$  as we can verify in Fig.6 for the blue shifted  $\langle R \rangle_{\text{bgcp}}$  evaluating  $\langle R \rangle$  at  $\hbar\omega = 1.97, 2.19, 2.3$  and  $2.4$  eV corresponding to increasing  $\theta = 9^\circ, 10^\circ, 10.5^\circ$  and  $11^\circ$ , respectively but using  $\lambda = 1239.8/\hbar\omega$ . Thus, It is interesting to note that  $\langle R \rangle_{\text{bgcp}}$  changes from  $\lambda_r = 629.3$  nm at  $\theta = 9^\circ$  to  $\lambda_g = 514.9$  nm at  $\theta = 11^\circ$  displaying a change from red to green colors with smalls changes of  $\theta$ .

## 4 Conclusions

In this work we have calculated using `Photonic`[18] the anisotropic macroscopic dielectric tensor of a layer we used to model the anisotropic reflectance of the Bouligand structures [13] for cuticle made of stratified chitin microfilamentary particles. We have explored anisotropy of the macroscopic dielectric tensor taken into account the chitin particles geometry, lattice arrangement, aspect ratio and the filling fractions. We have considered the Bouligand cuticle structure that are characterized by rotated layers of thickness  $d$  developing helical structure with pitch  $p = 360d/\theta$  and  $\theta$  the rotation angle between two consecutive layer that constitute the entire cuticle structure. To take into account the cuticle anisotropic reflectance we have calculated the dielectric tensor of each rotated layer in the laboratory frame and we have introduced a transfer matrix method of  $4 \times 4$  components that allows translate self consistently from above to below the incident electromagnetic fields on the Bouligand structure. We found that for no polarized light a reflectance band gap develops with a centroid position  $\langle R \rangle_{\text{bgcp}}$  in agreement with the expected constructive interference Eq.(19) relation. These reflectance band gap can be seen as the superposition of the two orthogonal responses in the laboratory frame  $R_{xx}$  and  $R_{yy}$ . We show that  $\langle R \rangle_{\text{bgcp}}$  is larger when  $\Delta n$  increases and that  $\Delta n$  is very sensitive to the particle geometry and lattice arrangement. These facts were also noticed by many authors [12] but anybody overcame the challenge to calculate cuticle optical responses considering the chitin particle geometry, lattice arrangement and filling fractions up to now. Also, we analyses the reflectance dependencies on the  $\theta$  angle that control the helix pitch  $p$  of the helical cuticle structure through  $p = 360d/\theta$ . We show how the ripples shape of  $\langle R \rangle_{\text{bgcp}}$  [12] can arise from unbalanced contribution of orthogonal components when  $\theta$  is not commensurable with some integer of the full helix rotation. We found that shifts to blue of  $\langle R \rangle_{\text{bgcp}}$  proportionally to  $\theta$  increases as we can expect from the decrease of  $p$  and Eq.(19) promoting structural color to changes from red to blue by relatively small changes in  $\theta$ .

## Acknowledgment

GPO thanks to SGCyT-UNNE for financial support through grant PI18F008. WLM thanks DGAPA-UNAM for support through grant IN109822.

## References

- [1] A.C.Neville and S.Caveney. Scarabaeid beetle exocuticle as an optical analogue of cholesteric liquid crystals. *Biol. Rev. Camb. Philos. Soc.*, 44:531–562, 1969.
- [2] Andrew R. Parker, David R. McKenzie, and Maryanne C. J. Large. Multilayer reflectors in animals using green and gold beetles as contrasting examples. *Journal of Experimental Biology*, 201(9):1307–1313, 05 1998.
- [3] Jeremy W. Galusha, Lauren R. Richey, John S. Gardner, Jennifer N. Cha, and Michael H. Bartl. Discovery of a diamond-based photonic crystal structure in beetle scales. *Phys. Rev. E*, 77:050904, May 2008.

- [4] Vivek Sharma, Matija Crne, Jung Ok Park, and Mohan Srinivasarao. Structural origin of circularly polarized iridescence in jeweled beetles. *science*, 325(5939):449–451, 2009.
- [5] Anthony C. Neville. *Biology of the Arthropod Cuticle*. Springer-Verlag, 1975.
- [6] Ana Luna, Demetrio Macías, Diana Skigin, Marina Inchaussandague, Daniel Schinca, Miriam Gigli, and Alexandre Vial. Characterization of the iridescence-causing multilayer structure of the ceroglossus suturalis beetle using bio-inspired optimization strategies. *Opt. Express*, 21(16):19189–19201, Aug 2013.
- [7] P.J. Gullan and P.S. Cranston. *The Insects: An Outline of Entomology*. J. Wiley & Sons, Ltd., Oxford, UK, fifth edition, 2014.
- [8] Andrew Richard Parker. 515 million years of structural colour. *Journal of Optics A: Pure and Applied Optics*, 2(6):R15, nov 2000.
- [9] T. Lenau and M. Barfoed. Colours and metallic sheen in beetle shells — a biomimetic search for material structuring principles causing light interference. *Advanced Engineering Materials*, 10(4):299–314, 2008.
- [10] Anthony Charles Neville. *Biology of Fibrous Composites: Development beyond the Cell Membrane*. Cambridge University Press, 1993.
- [11] J. David Pye. The distribution of circularly polarized light reflection in the scarabaeoidea (coleoptera). *Biological Journal of the Linnean Society*, 100(3):585–596, 2010.
- [12] I. E. Carter, K. Weir, M. W. McCall, and A. R. Parker. Variation in the circularly polarized light reflection of Lomaptera (Scarabaeidae) beetles. *Journal of The Royal Society Interface*, 13(120), 2016.
- [13] Y. Bouligand. Twisted fibrous arrangements in biological materials and cholesteric mesophases. *Tissue and Cell*, 4(2):189–217, 1972.
- [14] Sharon A. Jewell, Peter Vukusic, and Nicholas W. Roberts. Circularly polarized colour reflection from helicoidal structures in the beetle plusiotis boucardi. *New Journal of Physics*, 9:99 – 99, 2007.
- [15] E.Hecht and A.Zajac. *Optica*. Addison-Wesley Iberoamericana, S.A., 1986.
- [16] M.W. McCall, I.J. Hodgkinson, and Q. Wu. *Birefringent Thin Films and Polarizing Elements*. Imperial College Press, London, second edition, 2015.
- [17] Rudolf Oldenbourg and Teresa Ruiz. Birefringence and macromolecules wiener’s theory revisited, with application to dna and tobacco mosaic virus. *Biophys. J.*, 56:195–205, 1989.
- [18] W. Luis Mochán, Guillermo Ortiz, Bernardo S. Mendoza, and José Samuel Pérez-Huerta. Photonic. Comprehensive Perl Archive Network (CPAN), 2016. Perl package for calculations on metamaterials and photonic structures.

- [19] M. Born and E. Wolf. *Principles of Optics*. Cambridge University Press, seven edition, 1999.
- [20] Leandro L. Missoni, Guillermo P. Ortiz, María Luz Martínez Ricci, Victor J. Toranzos, and W. Luis Mochán. Rough 1d photonic crystals: A transfer matrix approach. *Optical Materials*, 109:110012, 2020.
- [21] Luis Eduardo Puente-Díaz, Victor Castillo-Gallardo, Guillermo P. Ortiz, José Samuel Pérez-Huerta, Héctor Pérez-Aguilar, Vivechana Agarwal, and W. Luis Mochán. Stable calculation of optical properties of large non-periodic dissipative multilayered systems. *Superlattices and Microstructures*, 145:106629, 2020.
- [22] Pochi Yeh. *Optical Waves in Layered Media*. Wiley Series in Pure and Applied Optics. Wiley, Hoboken, New Jersey, USA, 2005.